Solar Energy Materials & Solar Cells 298 (2026) 114149

Contents lists available at ScienceDirect

Solar Energy Materials and Solar Cells

journal homepage: www.elsevier.com/locate/solmat

Charge trapping, hydrogen accumulation, and structural rearrangement: A complete model for ultraviolet-induced degradation in TOPCon devices

Muhammad Umair Khan [a,*], Alison Ciesla [a], Aeron Johns [a], Chandany Sen [a], Ting Huang [b], Hao Song [b], Munan Gao [b], Ruirui Lv [b,**], Yuanjie Yu [b], Xinyuan Wu [a], Haoran Wang [a], Xutao Wang [a], Bram Hoex [a,***]

[a] School of Photovoltaic and Renewable Energy Engineering, University of New South Wales, Sydney, Australia, 2052
[b] Canadian Solar Inc., Suzhou, Jiangsu, 215129, China

A B S T R A C T

Tunnel oxide passivated contact (TOPCon) solar cells are susceptible to ultraviolet (UV)-induced degradation (UVID), which reduces their long-term performance. This study investigates the UVID mechanism in TOPCon lifetime structures with thin (4 nm) and thick (7 nm) AlO_x layers. We use a cycle of UV exposure, dark storage, and dark annealing to track changes in chemical and field-effect passivation. During UV exposure, the chemical passivation degrades, shown by an increase in the interface defect density (D_{it}). We attribute this to high-energy UV photons breaking Si-H bonds within the SiN_x capping layer, which releases mobile hydrogen that subsequently accumulates at the interface, thereby causing recombination-active defects. In contrast, the field-effect passivation is temporarily enhanced by charge trapping in the AlO_x, which increases its negative fixed charge (Q_f). A subsequent "dark storage degradation" occurs as these charges de-trap, while the chemical damage remains unchanged. During dark annealing, the accumulated hydrogen at the interface diffuses into the silicon bulk. This reduction in interfacial hydrogen concentration restores surface chemical passivation, as confirmed by a decrease in D_{it}. Although the chemical passivation shows a full recovery, as confirmed by a decrease in D_{it}, the FTIR analysis reveals that the complete degradation and recovery cycle induces a permanent structural rearrangement of the dielectric stack. Furthermore, the results show that the thicker 7 nm AlOx layer provides better UVID resilience. Since the field-effect passivation behaves similarly for both thicknesses, we attribute this resilience to the thicker film acting as a more effective physical barrier, reducing the transport of mobile hydrogen to the interface. This work presents a comprehensive model that links the observed UVID to specific, underlying structural changes in the passivation stack, providing guidance to address this failure mode at the solar cell level.

1. Introduction

Recent studies have highlighted the significant vulnerability of modern high-efficiency solar cells to ultraviolet-induced degradation (UVID) [1–4], a degradation mode of increasing relevance due to the widespread adoption of UV-transparent encapsulants in photovoltaic modules [5]. UVID is shown to deteriorate the interface passivation quality, and studies have consistently demonstrated reductions in open-circuit voltage (V_{oc}) and overall cell efficiency [2,4,6,7]. While standard qualification tests (e.g., IEC 61215 [8]) utilise a broad UV spectrum (280–400 nm), our previous work demonstrated that UVID in these structures is strongly wavelength-dependent and primarily driven by high-energy photons [4]. The dissociation of Si-H bonds requires photon energies greater than ~3.4 eV (wavelengths <365 nm) [9]. Therefore, this study uses a UV-B source to specifically accelerate this mechanism, allowing for a detailed kinetic analysis of UVID that would be significantly slower under broad-spectrum illumination.

The commercially dominant Tunnel-oxide passivated contact (TOPCon) cell technology is especially vulnerable to UVID [5]. TOPCon has surpassed the Passivated Emitter and Rear Contact (PERC) cell and dominates the current photovoltaic market due to its improved efficiency [10,11]. In addition to its polysilicon on oxide passivating contact at the rear, a TOPCon solar cell relies on an advanced front-side passivation stack composed of an AlO_x layer capped by a SiN_x layer [11–13]. This stack achieves extremely low interface recombination and maximises cell efficiency through two mechanisms: chemical passivation and field-effect passivation [13–15]. Chemical passivation reduces the density of interface defects (D_{it}) [16,17], while field-effect passivation arises from a large negative fixed charge (Q_f) within the AlO_x layer that repels electrons from the surface [17–19]. It has been identified that

* Corresponding author.
** Corresponding author.
*** Corresponding author.
E-mail addresses: m.umair@unsw.edu.au (M.U. Khan), ruirui.lv@csisolar.com (R. Lv), b.hoex@unsw.edu.au (B. Hoex).

https://doi.org/10.1016/j.solmat.2025.114149
Received 12 October 2025; Received in revised form 19 December 2025; Accepted 29 December 2025
Available online 5 January 2026

UVID in TOPCon is strongly dependent on the specific passivation properties [20–22], such as the aluminium oxide (AlO_x) and silicon nitride (SiN_x) layers that are the focus of this work.

In-depth investigations into UVID in such AlO_x/SiN_x passivated structures suggest a complex interplay of phenomena impacting both chemical and field-effect passivation [3,9]. The fundamental cause of degradation is understood to be the interaction of high-energy UV photons with the hydrogen-rich dielectric layers [3,19]. It is well-established that photons with energies greater than the Si-H bond energy (~3.4 eV) can break these bonds [9,23]. This dissociation creates two direct consequences: mobile atomic hydrogen and recombination-active silicon dangling bonds at the interface [9]. The creation of these dangling bonds is the direct physical cause for the increase in interface defects [19,23,24]. The process is further complicated by a phenomenon known as "dark storage degradation," where the passivation quality continues to degrade after the UV exposure [9,25]. This effect, observed in AlO_x passivated silicon, manifests as a slow decay of the effective carrier lifetime over hours to days when the sample is stored in darkness after being illuminated [21]. While this slow degradation is thought to be caused by the slow de-trapping of charges from the AlO_x layer [24], the precise kinetics of this process and its direct correlation to structural changes in the passivation stack are not well understood, presenting a key knowledge gap in predicting the long-term stability of these devices. Finally, although it is known that degradation can be partially reversed through a thermal annealing step, the precise recovery mechanism remains a topic of debate.

This study aims to explain the underlying mechanisms behind UVID in TOPCon structures. By applying advanced characterisation techniques, including Corona-Oxide Characterisation of Semiconductors (COCOS) and Fourier-transform infrared spectroscopy (FTIR), our study investigates changes in D_{it} and Q_f under controlled UV exposure, dark storage, and thermal annealing conditions and relates them to structural changes in the dielectric stack. By varying the thickness of AlO_x (4 nm vs. 7 nm) and assessing structures with and without emitters, we comprehensively characterise the interplay between chemical and field-effect passivation. The findings reveal a complex interplay between chemical degradation and a temporary, charge-trapping-induced enhancement in field-effect passivation, which is followed by a metastable decay in the dark. This detailed approach offers practical insights into designing more robust, UV-resistant photovoltaic technologies that can maintain sustained performance in harsh operational environments.

2. Experimental details

Symmetrical lifetime structures were fabricated on n-type Czochralski (Cz) silicon wafers on an industrial manufacturing line. The fabrication process began with saw damage etching and texturing, followed by an alkaline chemical polish to remove the texture on both sides. The first set (SP1 and SP2) was processed without a diffused emitter, allowing for direct measurement of passivation quality via COCOS. The second set (SP3 and SP4) included a boron-diffused emitter with a sheet resistance of 400 Ω/□ to represent the structure of a finished cell's front side. The primary passivation stack was then deposited, consisting of an AlO_x layer grown by atomic-layer deposition (ALD, Leadmicro, KF20000) and a 75 nm SiN_x capping layer deposited by plasma-enhanced chemical vapour deposition (PECVD, Shenzhen S. C, 520max). The AlO_x layer thickness was varied between two conditions: a thin 4 nm film and a thicker 7 nm film. These values were selected based on the standard industrial processing window for TOPCon front-side passivation. The 4 nm thickness (samples SP1, SP3) represents a cost-effective minimum used in industry, while the 7 nm thickness (samples SP2, SP4) is still sufficiently thin to not significantly affect the optical properties of the dielectric stack. This comparison allows for the assessment of the trade-off between manufacturing throughput and UVID resilience. Due to the automated manufacturing environment, these wafers exhibit high homogeneity. The typical experimental uncertainty for the lifetime measurements is ±10 %, which is negligible compared to the magnitude of the UV-induced degradation effects observed. Fig. 1 illustrates the schematic of the symmetrical test structures used in this study.

Following fabrication, the wafers were cleaved into 4 cm × 4 cm tokens. The experimental procedure was designed to systematically degrade and recover the samples, consisting of three primary stages. First, the UV degradation tests were conducted using USHIO G8T5E UV-B lamps with a spectral peak centred at 313 nm. The samples were placed in a temperature-controlled chamber maintained at 60 °C. The spectral irradiance was characterised using a calibrated spectroscopy system comprising an Avantes AvaSpec ULS4096CL-EVO spectrometer connected to a 550 μm core optical fibre equipped with an SMA cosine corrector. The measurement system was calibrated against a NIST-traceable balanced halogen/deuterium source (Avalight-DH-S-BAL). The absolute UV intensity was determined by integrating the spectral irradiance over the relevant bandwidth and was maintained at 112 W/m^2 at the sample surface. The samples were exposed to UV radiation without a cover glass. This setup was selected to accelerate the degradation and to directly investigate the stability of the dielectric stack against high-energy UV photons. The samples were subjected to UV-B radiation for a total dose of 14.3 kWh/m^2 [4]. This dose was selected to achieve a significant level of UVID and was not based on a standard (e.g., IEC 671215). This allowed us to characterise the underlying chemical and structural changes in the passivation stack. Second, to investigate the stability of passivation after illumination, the samples were stored in the dark at ambient temperature for two weeks. Third, a recovery phase was initiated by performing a dark anneal (DA) at 85 °C in the absence of any light.

The passivation quality and structural properties were monitored throughout the experiment using advanced characterisation techniques performed at each key stage, as illustrated in the experimental workflow in Fig. 2: before the initial UV exposure, after UV exposure, after dark storage, and after thermal annealing. The effective minority carrier lifetime (τ_{eff}) was measured using a Sinton Instruments WCT-120TS tool in quasi-steady-state photoconductance (QSS-PC) mode. The effective lifetime values were determined from the photoconductance decay curves using the transient method, with a correction for intrinsic recombination applied using the Richter model [26]. The J_{0e} was extracted from the injection-dependent lifetime data using the Kane-Swanson method [27,28]. The slope was fitted in the high-injection regime. The background doping concentration used for this analysis was derived from the measured base resistivity of the n-type Cz silicon wafers. To quantify the contributions from chemical and field-effect passivation, COCOS was employed on the non-emitter samples (SP1, SP2). The COCOS technique deposits a controlled amount of charge onto the dielectric surface using a corona discharge, while a non-contact Kelvin probe measures the resulting surface potential in the dark and under illumination. By analysing the surface photovoltage (SPV) response to dark and illumination, both the Q_f and the D_{it} can be extracted. Following each COCOS analysis, samples were rinsed with deionised (DI) water. This step is essential to neutralise and remove the corona charge deposited on the SiN_x capping layer during measurement. This ensures that the surface potential is "reset" without altering the Q_f or D_{it}, as the SiN_x stable capping layer protects the underlying passivation stack from the rinsing process. Finally, to study structural changes within the dielectric layers, FTIR measurements were performed using a p-polarised infrared beam at an angle of incidence of approximately 74°. This setup, corresponding to Brewster's angle for silicon, minimises reflection, which suppresses undesired optical interference fringes and maximises measurement sensitivity to the vibrational modes within the thin AlO_x and SiN_x layers [29]. To isolate the absorbance signature of the thin passivation films from that of the bulk silicon wafer, a reference spectrum was obtained from a bare silicon wafer from the same batch with no dielectric films. This reference spectrum was then subtracted from all subsequent sample measurements, effectively removing the

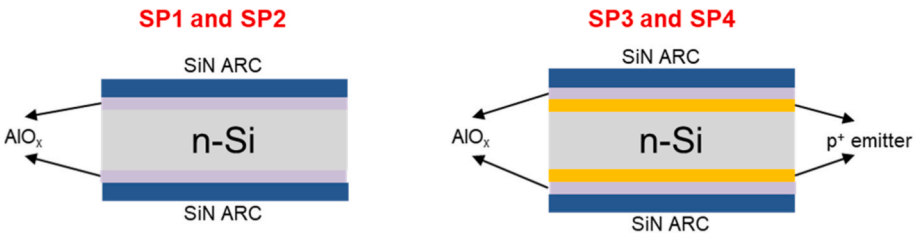

Fig. 1. Schematic of the symmetrical test structures used in this study. (a) Non-emitter structures (SP1 and SP2). (b) Emitter-containing structures (SP3 and SP4).

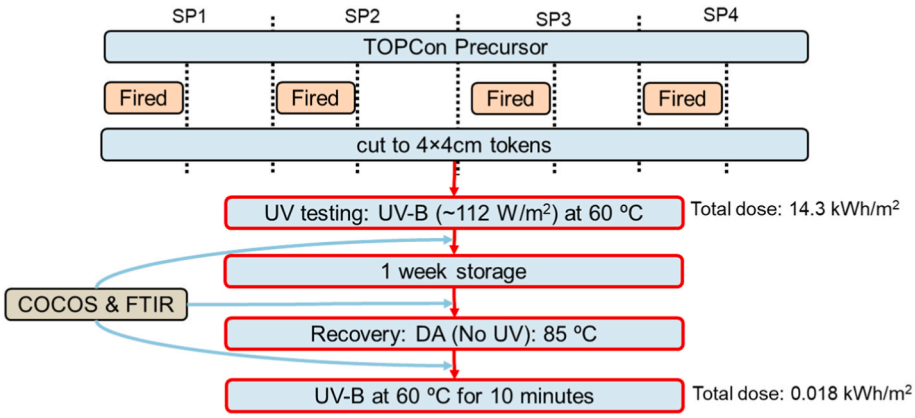

Fig. 2. Schematic of the experimental workflow with periodic characterisations to study UV impact on TOPCon.

contribution from the silicon substrate and ensuring that the final spectra represent only the absorption due to the passivation stack.

3. Results & discussion

The impact of UV exposure on the passivation quality of the TOPCon precursors is presented in Fig. 3, which plots the emitter saturation current density (J_{0e}) as a function of UV dose for all sample sets. Across all tested structures, a clear increase in J_{0e} was observed with increasing UV dose, indicating degradation of the surface passivation. The data reveals two critical trends related to the sample processing and structure. Firstly, while both fired and non-fired samples degrade, the fired samples consistently exhibit less degradation and superior UVID resilience compared to their non-fired samples across all groups. Secondly, the AlO_x layer thickness is a dominant parameter in showing the degradation trend. This is clearly visible in both the non-emitter (Fig. 3 (a)) and emitter-containing (Fig. 3(b)) samples, where the structures with the thinner 4 nm AlO_x layer (SP1 and SP3) consistently degrade more severely than those with the thicker 7 nm AlO_x layer (SP2 and SP4). The finding that a thicker AlO_x layer provides greater stability is consistent with previous reports for AlO_x/SiN_x stacks under thermal and UV stress [22].

The complete degradation and recovery cycle is presented in Fig. 4, which plots the evolution of the emitter saturation current density (J_{0e}) through the three experimental stages: UV exposure, dark storage, and thermal recovery. The initial UV Exposure phase (as shown in Fig. 3) reveals the trends observed previously, with thin AlO_x samples (SP1 and SP3) exhibiting the most rapid degradation. Notably, the subsequent "Dark Storage" period shows that the degradation persists and, for the most unstable samples, accelerates significantly after the UV source is removed. This secondary, surface-related degradation is not uniform, as its magnitude varies for different samples. Unlike the initial UV degradation, there is no clear pattern correlating the extent of the dark storage degradation with the thickness of the AlO_x layer. For all samples, the degradation continued for a two-week storage period. Finally, the dark annealing stage demonstrates a rapid and substantial reduction in J_{0e}. This confirms that the decrease in interface passivation caused by the UVID process is metastable and can be effectively reversed through a

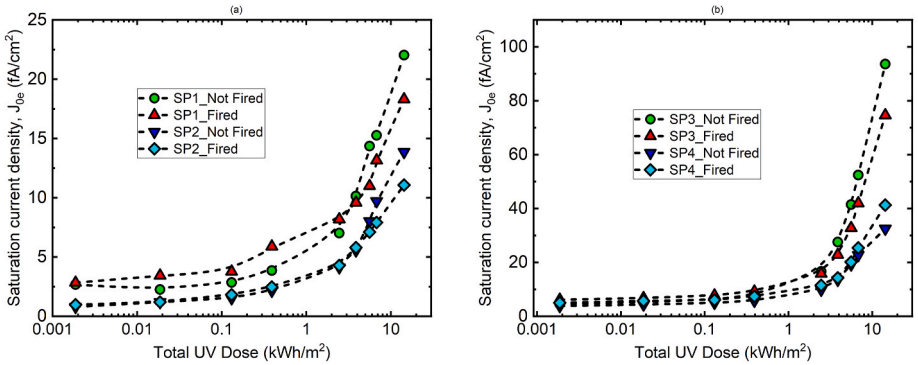

Fig. 3. Emitter saturation current density (J_{0e}) as a function of total UV-B dose for (a) non-emitter samples and (b) emitter-containing samples. The data compares samples with a thin (4 nm, SP1 and SP3) and thick (7 nm, SP2 and SP4) AlO_x layer, both before and after a firing step.

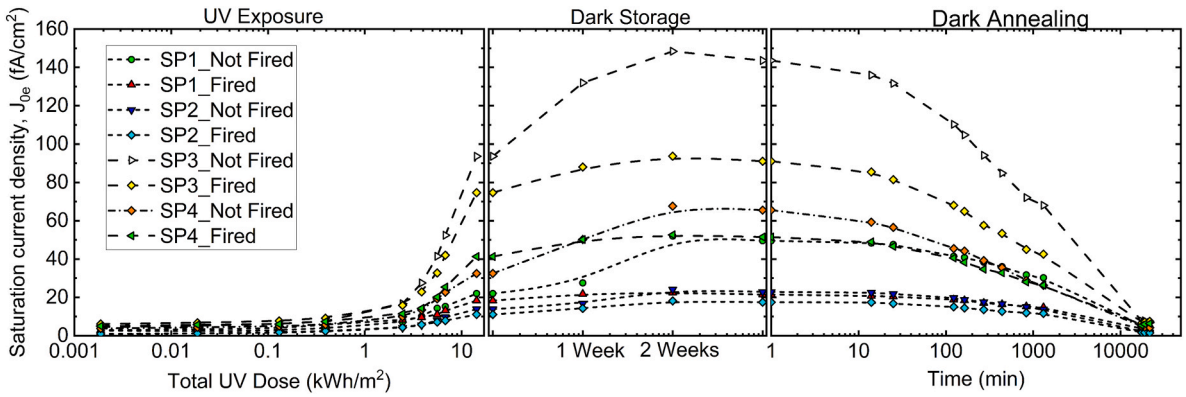

Fig. 4. Change in the emitter saturation current density (J_{0e}) throughout the experimental sequence showing initial degradation during UV exposure, the subsequent dark storage degradation, and the final thermal recovery during dark annealing.

low-temperature thermal treatment, with all samples returning to J_{0e} values similar to those at the start of the experiment.

To study the passivation mechanisms, the change in D_{it}, a direct measure of chemical passivation quality, was measured at each stage of the experiment, as shown in Fig. 5. The data show that the initial UV exposure causes an increase in D_{it} for all sample groups. During the subsequent one-week dark storage period, the D_{it} remains relatively unchanged. This is an important finding, as it implies that the dark storage degradation observed in the overall J_{0e} is not caused by a further increase in D_{it}, but originates from a different mechanism. Following the DA, which shows a significant reduction in D_{it} for all samples, the D_{it} is reduced to a value similar to the initial value at the start of the experiments. This provides strong evidence that the thermal treatment effectively repairs the interface by promoting the re-passivation of UV-induced defects. The behaviour of the D_{it}, showing an increase due to UV exposure, stability in the dark, and a reduction with thermal annealing, confirms that degradation of chemical passivation is a reversible component of the UVID mechanism.

The corresponding changes in field-effect passivation were evaluated by measuring Q_f, with the results presented in Fig. 6. UV exposure leads to an increase in field-effect passivation, as the negative Q_f increases for all sample groups. During the subsequent one-week dark storage, the negative Q_f decreases to its initial state. Concurrent with the recovery in chemical passivation (the decrease in D_{it}), the negative Q_f decreases to a value that is significantly lower than at the start of the experiment. However, after the subsequent short UV exposure, the negative Q_f increases, similar to the first UV exposure.

To investigate the structural origin of the observed changes, FTIR measurements were performed. A representative deconvoluted spectrum is shown in Fig. 7(a), identifying the primary vibrational modes attributed to Si-N bonds (Peak 1, ~816 cm^{-1}), complex Si-O-N bonds (Peak 2, ~924 cm^{-1}), and the main Si-O-Si bonds of the interfacial oxide (Peak 3, ~1090 cm^{-1}, and its longitudinal optic mode, Peak 4, ~1193 cm^{-1}). The evolution of these peaks throughout the experiment is summarised in Fig. 7(b). The data show that the area of Peak 1 (Si-N) decreases after the initial UV exposure and continues to decrease following the recovery anneal. In contrast, Peak 2 (Si-O-N) shows no significant change in its area but exhibits a significant and continuous shift to a higher wavenumber, mainly changing during UV exposure and the dark annealing stage. While the main Si-O-Si peak (Peak 3) remains stable, Peak 4 (the Si-O-Si LO mode) also shows a clear and continuous shift to a higher wavenumber. Physically, a shift to a higher wavenumber indicates a strengthening of the bond and a relaxation of the bond angle. In this context, it confirms a densification of the interfacial

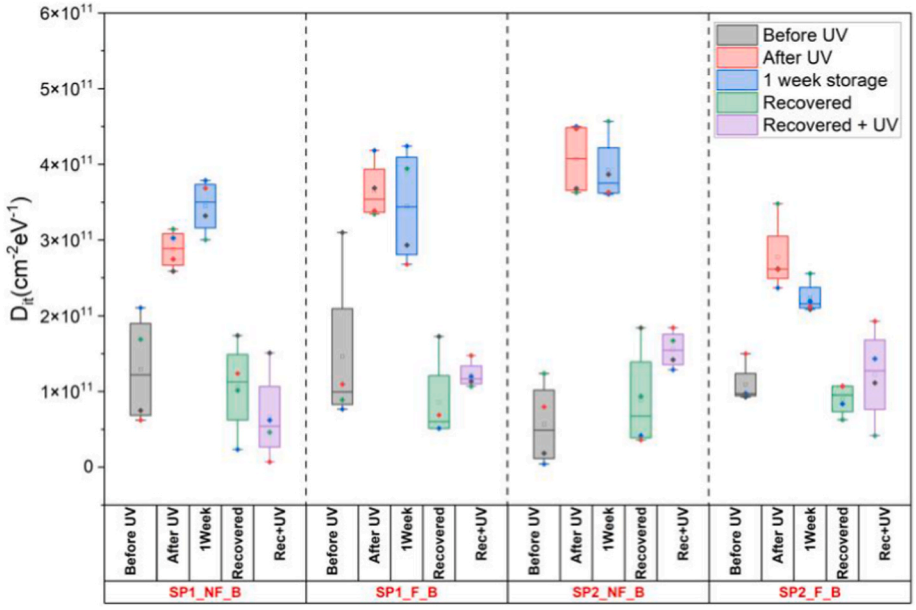

Fig. 5. Interface defect density (D_{it}) for non-emitter sample structures at each stage of the experiment, including before UV, after UV, after storage, and after a short UV exposure, extracted from COCOS measurements.

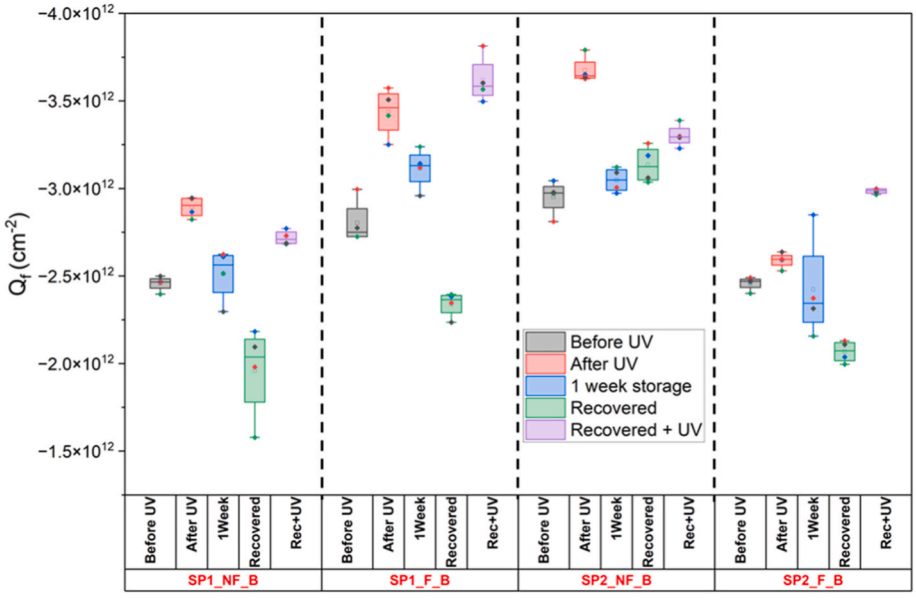

Fig. 6. Fixed charge density (Q_f) for non-emitter sample structures measured via COCOS at each stage of the experiment. The data distinguishes between thin 4 nm AlO_x (SP1) and thick 7 nm AlO_x (SP2) samples, in both Non-Fired (NF) and Fired (F) conditions.

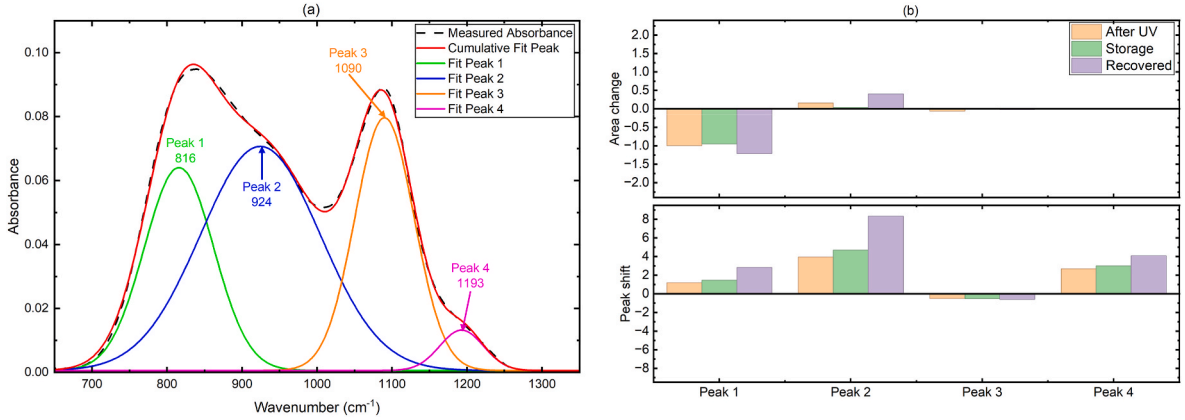

Fig. 7. Analysis of the passivation stack by FTIR performed on the SP4_F sample (7 nm AlO_x, Fired). (a) A representative deconvoluted FTIR spectrum showing the primary vibrational modes. (b) Summary of the relative area change and peak shift for each deconvoluted peak at different stages of the experiment.

oxide, suggesting that the layer transforms into a more stable, ordered structure during the degradation and recovery cycle.

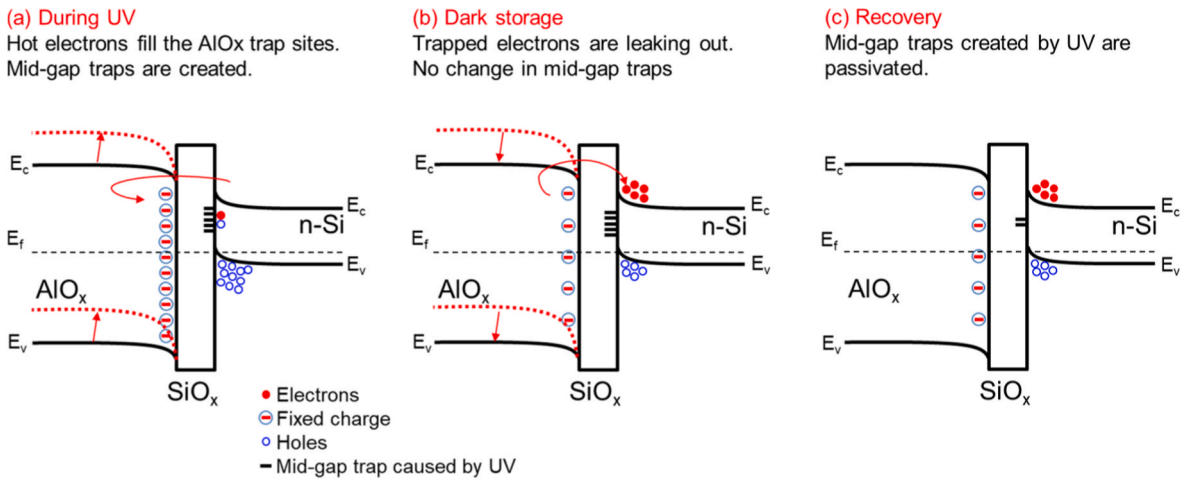

Fig. 8. Schematic of the proposed UVID mechanism in the passivation stack (a) during UV exposure, (b) during dark storage, and (c) after the thermal anneal.

3.1. Proposed UVID mechanism

The combined experimental results enable the construction of a comprehensive model for the UVID mechanism, as illustrated in Fig. 8. The initial degradation process during UV exposure, illustrated in Fig. 8 (a), is a complex interplay between competing phenomena that simultaneously degrade the chemical passivation while enhancing the field-effect passivation. The foundational cause is the breaking of Si-H bonds within the SiN_x:H capping layer by high-energy UV photons. This dissociation releases a high concentration of mobile hydrogen into the stack. While the mobile hydrogen species itself is not directly visible in standard FTIR, the spectral analysis confirms the structural breakdown of the layer: the permanent reduction in the Si-N peak area (Peak 1) [Fig. 7(b)] indicates the concurrent oxidation and destabilisation of the SiN_x framework. This structural degradation facilitates the release and transport of hydrogen to the interface. The mechanism of hydrogen redistribution is well-supported by our recent studies [2,4,30], where ToF-SIMS depth profiling directly confirmed the accumulation of hydrogen at the interface following UV exposure in identical TOPCon structures. The results of the current study align with this model: the FTIR data confirms the permanent structural degradation of the SiN_x layer, while the reversible evolution of D_{it} provides the electrical signature of the hydrogen accumulation and subsequent passivation at the interface, which leads to the formation of new recombination-active defects [2,4]. Specifically, excess interfacial H forms fragile Si–H_2/H_3 and H-decorated oxygen vacancy complexes, introducing mid-gap states that cause recombination activity [31,32]. This degradation of the chemical passivation is confirmed by the measured increase in D_{it} shown in Fig. 5. In parallel with this chemical degradation, a separate electronic process occurs where UV-generated "hot electrons" from the silicon are injected into the AlO_x layer. This charge trapping [19,24], confirmed by the increase in the negative Q_f shown in Fig. 6, improves the field-effect passivation. This model, centred on the transport of mobile hydrogen, also explains the key trends observed in the lifetime data in Fig. 3. Firstly, the thicker (7 nm) AlO_x layer provides better UVID resilience because it is a more effective barrier, reducing the amount of mobile hydrogen reaching the interface. Secondly, the fired samples consistently show less degradation, which can be attributed to two concurrent effects from the high-temperature process. This could be due to the lower hydrogen content of the SiN_x film after firing, thus reducing the amount of mobile hydrogen generated during UVID, or due to densification of the interfacial silicon oxide layer.

The second stage of the mechanism, illustrated in Fig. 8(b), occurs during dark storage, where the J_{0e} increases despite the absence of UV light. The chemical and structural changes caused by UV exposure remain stable during dark storage. This is confirmed by two key observations: the D_{it} remains high and unchanged, as shown in Fig. 5, and the FTIR spectra show no significant evolution in the interfacial bonds (Fig. 7). The continued increase in J_0 in Fig. 4 is therefore attributed to the detrapping of negative fixed charge from the AlO_x layer, similar as that observed by Gielis et al. using *in situ* electric field induced second harmonic generation [19]. This charge de-trapping is directly observed as a decrease in the Q_f in Fig. 6. The reduction in field-effect passivation, while the chemical passivation remains constant, explains the "dark storage degradation" phenomenon.

The final stage of the mechanism, illustrated in Fig. 8(c), is the dark anneal. The redistribution of hydrogen is at the centre of this process. The thermal energy provides the mobility for the excess hydrogen accumulated at the interface to diffuse into the bulk silicon. Firstly, it recovers the chemical passivation by reducing the defect-rich environment, leading to the reduction in D_{it}, as seen in Fig. 5. Secondly, the thermal treatment induces relaxation of the AlO_x layer, leading to a reduction in the measured Q_f in Fig. 6. This reduction in Q_f is accompanied by a significant decrease in D_{it}. Since high D_{it} can result in interface trapped charge (Q_{it}) that partly mirrors fixed charge, the simultaneous reduction of both parameters indicates a restoration of the interface quality and a stabilisation of the band bending. Finally, the short UV exposure applied after recovery causes the negative Q_f to rapidly increase (Fig. 6). This demonstrates that the trap-filling kinetics are fast, as only a small UV dose is required to saturate the available trap states within the AlO_x layer. Prolonged exposure beyond this point does not yield a further increase in fixed charge, explaining why the short second dose results in Q_f values comparable to the long initial exposure. Notably, the FTIR analysis in Fig. 7 confirms that this electronic recovery is accompanied by a permanent structural transformation of the passivation stack. The data show that the area of the Si-N peak (Peak 1) continues to decrease during the anneal, indicating an irreversible rearrangement and densification of the SiN_x film. Simultaneously, the Si-O-N peak (Peak 2) increases in intensity and shifts to a higher wavenumber which is attributed to the oxidation of the top surface of the SiN_x layer [33]. Although this represents a permanent chemical modification of the passivation stack, it is confined to the SiN_x surface and is therefore not regarded as being directly linked to the electronic changes at the AlO_x/SiO_x/p^+-Si interface. The Si-O-Si peak (Peak 3) exhibits a shift to a higher wavenumber after the thermal anneal. This shift is an indicator of the densification of the interfacial SiO_x layer, as it reflects a relaxation of the Si-O-Si bond angles towards a more ordered, stable state [34]. While the passivation quality is restored using DA, the FTIR analysis confirms that the passivation stack is permanently changed.

4. Conclusion

This study systematically investigated the mechanisms of UVID in TOPCon lifetime structures, revealing a complex, metastable process. The results demonstrate that UVID is a complex, metastable process that impacts the properties of both chemical and field-effect passivation. During UV exposure, mobile hydrogen is released in the SiN_x capping layer by the breaking of Si-H bonds. This mobile hydrogen accumulates at the interface, thereby increasing the D_{it}. Simultaneously, a separate process of charge trapping temporarily improves field-effect passivation by increasing the negative Q_f. Subsequently, a 'dark storage degradation' occurs as trapped charge is released (de-trapping), while the underlying chemical damage remains unchanged. Finally, a low-temperature dark anneal redistributes the mobile hydrogen at the interface, which simultaneously reduces D_{it} and alters the baseline Q_f.

These electronic changes are accompanied by permanent structural modifications, as confirmed by FTIR analysis. The results show that the complete degradation and recovery cycle induces an irreversible structural rearrangement of the SiN_x capping layer and a chemical transformation and densification of the interfacial oxide layer. This comprehensive model, linking electronic degradation to specific structural changes, also confirms that a thicker (7 nm) AlO_x layer provides superior UVID resilience by acting as a more effective barrier to the detrimental transport of mobile hydrogen. These results provide important guidance for designing more durable passivation layers and refining accelerated testing protocols to secure the long-term reliability of TOPCon technology. The work establishes a comprehensive model connecting UVID to specific structural changes in the passivation stack, offering a pathway to mitigate this failure mode at the cell level.

CRediT authorship contribution statement

Muhammad Umair Khan: Writing – review & editing, Writing – original draft, Visualization, Validation, Resources, Methodology, Investigation, Formal analysis, Data curation, Conceptualization. **Alison Ciesla:** Visualization, Supervision, Methodology, Investigation, Data curation. **Aeron Johns:** Investigation, Data curation. **Chandany Sen:** Methodology, Investigation, Data curation. **Ting Huang:** Validation, Resources. **Hao Song:** Resources, Investigation. **Munan Gao:** Resources, Investigation. **Ruirui Lv:** Resources, Project administration, Investigation. **Yuanjie Yu:** Resources, Methodology. **Xinyuan Wu:** Validation, Investigation, Data curation. **Haoran Wang:** Visualization, Validation,

Data curation. **Xutao Wang:** Visualization, Validation, Data curation. **Bram Hoex:** Writing – review & editing, Visualization, Supervision, Project administration, Funding acquisition, Conceptualization.

Declaration of competing interest

The authors declare the following financial interests/personal relationships which may be considered as potential competing interests: Muhammad Umair Khan reports financial support was provided by Australian Renewable Energy Agency. Muhammad Umair Khan reports financial support was provided by Australian Centre for Advanced Photovoltaics. Muhammad Umair Khan reports financial support was provided by Trailblazer for Recycling and Clean Energy (TRaCE). If there are other authors, they declare that they have no known competing financial interests or personal relationships that could have appeared to influence the work reported in this paper.

Acknowledgement

This work was supported by the Australian Centre for Advanced Photovoltaics (ACAP) funded byAustralian Government through the Australian Renewable Energy (ARENA). The Australian Government does not accept the responsibility for the views, information, or advice expressed herein. The authors appreciate the support provided by the Australian Government's Trailblazer for Recycling & Clean Energy program, led by UNSW & the University of Newcastle. The authors extend their gratitude to the SLDOT team at SPREE UNSW, both at TETB and SIRF, for their invaluable support in upholding health and safety standards within the lab and ensuring the seamless operation of the facility, which facilitated the progress of our work.

Data availability

Data will be made available on request.

References

[1] R. Witteck, B. Veith-Wolf, H. Schulte-Huxel, A. Morlier, M.R. Vogt, M. Köntges, R. Brendel, UV-induced degradation of PERC solar modules with UV-transparent encapsulation materials, Prog. Photovoltaics Res. Appl. 25 (2017) 409–416, https://doi.org/10.1002/pip.2861.

[2] A. Sinha, J. Qian, S.L. Moffitt, K. Hurst, K. Terwilliger, D.C. Miller, L.T. Schelhas, P. Hacke, UV-induced degradation of high-efficiency silicon PV modules with different cell architectures, Prog. Photovoltaics Res. Appl. 31 (2023) 36–51, https://doi.org/10.1002/pip.3606.

[3] F.T. Thome, P. Meßmer, S. Mack, E. Schnabel, F. Schindler, W. Kwapil, M. C. Schubert, UV-Induced degradation of industrial PERC, TOPCon, and HJT solar cells: the next big reliability challenge? Sol. RRL (2024) https://doi.org/10.1002/solr.202400628.

[4] M.U. Khan, C. Sen, M. Pollard, T. Huang, M. Gao, R. Lv, Y. Yu, X. Wu, H. Wang, X. Wang, B. Hoex, UV-induced degradation in TOPCon solar cells: hydrogen dynamics and impact of UV wavelength, Sol. Energy Mater. Sol. Cell. 294 (2026), https://doi.org/10.1016/j.solmat.2025.113895.

[5] International Technology Roadmap for Photovoltaics (ITRPV), sixteenth ed., 2025. www.vdma.eu. (Accessed 2 October 2025).

[6] R. Witteck, B. Min, H. Schulte-Huxel, H. Holst, B. Veith-Wolf, F. Kiefer, M.R. Vogt, M. Köntges, R. Peibst, R. Brendel, UV radiation hardness of photovoltaic modules featuring crystalline Si solar cells with AlOx/p+-type Si and SiNy/n+-type Si interfaces, Phys. Status Solidi Rapid Res. Lett. 11 (2017), https://doi.org/10.1002/pssr.201700178.

[7] V. Guiheneuf, F. Delaleux, S. Pouliquen, O. Riou, P.O. Logerais, J.F. Durastanti, Effects of the irradiance intensity during UV accelerated aging test on unencapsulated silicon solar cells, Sol. Energy 157 (2017) 477–485, https://doi.org/10.1016/j.solener.2017.08.044.

[8] IEC, IEC 61215-1:2021, Terrestrial photovoltaic (PV) modules - design qualification and type approval. Part 1, Test Requirements, International Electrotechnical Commission, 2021.

[9] H. Ye, S. Huang, C. Qian, Z. Sun, Y. Chen, X. Song, Y. Zhang, N. Wang, Y. Hu, Y. Yang, L. Li, Z. Ma, T. Chen, W. Liu, J. Yu, Short wavelength photons destroying Si–H bonds and its influence on high-efficiency silicon solar cells and modules, Sol. RRL 7 (2023), https://doi.org/10.1002/solr.202300334.

[10] D. Yan, S.P. Phang, Y. Wan, C. Samundsett, D. Macdonald, A. Cuevas, High efficiency n-type silicon solar cells with passivating contacts based on PECVD silicon films doped by phosphorus diffusion, Sol. Energy Mater. Sol. Cell. 193 (2019) 80–84, https://doi.org/10.1016/j.solmat.2019.01.005.

[11] M.Q. Khokhar, H. Yousuf, S. Jeong, S. Kim, X. Fan, Y. Kim, S.K. Dhungel, J. Yi, A review on p-Type tunnel oxide passivated contact (TOPCon) solar cell, Transact.n Electr. Electr. Mater. 24 (2023) 169–177, https://doi.org/10.1007/s42341-023-00433-z.

[12] R.S. Bonilla, B. Hoex, P. Hamer, P.R. Wilshaw, Dielectric surface passivation for silicon solar cells: a review, Phys. Status Solidi (A) Appl. Mater. Sci. 214 (2017), https://doi.org/10.1002/pssa.201700293.

[13] B. Hoex, J. Schmidt, R. Bock, P.P. Altermatt, M.C.M. van de Sanden, W.M. M. Kessels, Excellent passivation of highly doped p-type Si surfaces by the negative-charge-dielectric Al2O3, Appl. Phys. Lett. 91 (2007), https://doi.org/10.1063/1.2784168.

[14] G. Dingemans, W.M.M. Kessels, Status and prospects of Al2O3-based surface passivation schemes for silicon solar cells, J. Vac. Sci. Technol. A: Vacuum Surf. Films 30 (2012), https://doi.org/10.1116/1.4728205.

[15] W. Li, Z. Xu, Y. Yan, J. Zhou, Q. Huang, S. Xu, X. Zhang, Y. Zhao, G. Hou, Passivating contacts for crystalline silicon solar cells: an overview of the current advances and future perspectives, Adv. Energy Mater. 14 (2024), https://doi.org/10.1002/aenm.202304338.

[16] S.W. Glunz, S. Rein, W. Warta, J. Knobloch, W. Wettling, Degradation of carrier lifetime in Cz silicon solar cells, Sol. Energy Mater. Sol. Cell. 65 (2001) 219–229, https://doi.org/10.1016/S0927-0248(00)00098-2.

[17] C. Battaglia, A. Cuevas, S. De Wolf, High-efficiency crystalline silicon solar cells: status and perspectives, Energy Environ. Sci. 9 (2016) 1552–1576, https://doi.org/10.1039/c5ee03380b.

[18] B. Hoex, S.B.S. Heil, E. Langereis, M.C.M. van de Sanden, W.M.M. Kessels, Ultralow surface recombination of c-Si substrates passivated by plasma-assisted atomic layer deposited Al2O3, Appl. Phys. Lett. 89 (2006), https://doi.org/10.1063/1.2240736.

[19] J.J.H. Gielis, B. Hoex, M.C.M. van de Sanden, W.M.M. Kessels, Negative charge and charging dynamics in Al2O3 films on Si characterized by second-harmonic generation, J. Appl. Phys. 104 (2008), https://doi.org/10.1063/1.2985906.

[20] R. Witteck, T. Dullweber, R. Brendel, H. Schulte-Huxel, P. Jager, M. Rudolph, H.-P. Sperlich, M. Konig, G. Kohler, D. Landgraf, H. Mehlich, M. Kontges, UV-stable surface passivation for crystalline silicon cells in solar modules with UV light transmitting encapsulation materials, in: 2019 IEEE 46th Photovoltaic Specialists Conference (PVSC), IEEE, 2019, pp. 2238–2242, https://doi.org/10.1109/PVSC40753.2019.8980612.

[21] G. Dingemans, P. Engelhart, R. Seguin, F. Einsele, B. Hoex, M.C.M. Van De Sanden, W.M.M. Kessels, Stability of Al2O3 and Al2O3/a- sinx:h stacks for surface passivation of crystalline silicon, J. Appl. Phys. 106 (2009), https://doi.org/10.1063/1.3264572.

[22] B. Veith-Wolf, R. Witteck, A. Morlier, H. Schulte-Huxel, M.R. Vogt, J. Schmidt, Spectra-dependent stability of the passivation quality of Al2O3/c-Si interfaces, IEEE J. Photovoltaics 8 (2018) 96–102, https://doi.org/10.1109/JPHOTOV.2017.2775147.

[23] T. Kamioka, D. Takai, T. Tachibana, T. Kojima, Y. Ohshita, Plasma damage effect on ultraviolet-induced degradation of PECVD sinx:h passivation, in: 2015 IEEE 42nd Photovoltaic Specialist Conference (PVSC), IEEE, 2015, pp. 1–3, https://doi.org/10.1109/PVSC.2015.7356326.

[24] B. Liao, R. Stangl, T. Mueller, F. Lin, C.S. Bhatia, B. Hoex, The effect of light soaking on crystalline silicon surface passivation by atomic layer deposited Al2O3, J. Appl. Phys. 113 (2013), https://doi.org/10.1063/1.4775595.

[25] P. Gebhardt, U. Kräling, E. Fokuhl, I. Hädrich, D. Philipp, Reliability of commercial TOPCon PV modules—an extensive comparative study, Prog. Photovoltaics Res. Appl. (2024), https://doi.org/10.1002/pip.3868.

[26] A. Richter, F. Werner, A. Cuevas, J. Schmidt, S.W. Glunz, Improved parameterization of auger recombination in silicon, Energy Proc. 27 (2012) 88–94, https://doi.org/10.1016/j.egypro.2012.07.034.

[27] T.U. Naerland, H. Haug, H. Angelskar, R. Sondena, E.S. Marstein, L. Arnberg, Studying light-induced degradation by lifetime decay analysis: excellent fit to solution of simple second-order rate equation, IEEE J. Photovoltaics 3 (2013) 1265–1270, https://doi.org/10.1109/JPHOTOV.2013.2278663.

[28] D. Kane, R. Swanson, Measurement of the emitter saturation current by a contactless photoconductivity decay method (silicon solar cells), in: IEEE Photovoltaic Specialists Conference, IEEE, 1985, pp. 578–583.

[29] C.Y. Lee, S. Deng, T. Zhang, X. Cui, K.T. Khoo, K. Kim, B. Hoex, Evaluating the impact of thermal annealing on c -Si/Al2O3 interface: correlating electronic properties to infrared absorption, AIP Adv. 8 (2018), https://doi.org/10.1063/1.5036738.

[30] D.C. Jordan, D.B. Sulas-Kern, S. Johnston, H.R. Moutinho, C. Xiao, C.S. Jiang, M. Young, A.G. Norman, C. Deline, I. Repins, R. Bhoopathy, O. Kunz, Z. Hameiri, C. Sainsbury, High efficiency silicon module degradation - from atoms to systems. www.nrel.gov/publications, 2020.

[31] E. Cartier, J.H. Stathis, D.A. Buchanan, Passivation and depassivation of silicon dangling bonds at the Si/SiO 2 interface by atomic hydrogen, Appl. Phys. Lett. 63 (1993) 1510–1512, https://doi.org/10.1063/1.110758.

[32] J.H. Stathis, E. Cartier, Atomic hydrogen reactions with Pb centers at the (100) Si/SiO2 interface, Phys. Rev. Lett. 72 (1994) 2745–2748, https://doi.org/10.1103/PhysRevLett.72.2745.

[33] T.D. To, A.T. Nguyen, K.N.T. Phan, A.T.T. Truong, T.C.D. Doan, C.M. Dang, Modification of silicon nitride surfaces with GOPES and APTES for antibody immobilization: computational and experimental studies, Adv. Nat. Sci. Nanosci. Nanotechnol. 6 (2015), https://doi.org/10.1088/2043-6262/6/4/045006.

[34] C.Y. Lee, S. Wang, X. Cui, T. Zhang, R. Deng, K.T. Khoo, B. Hoex, Improving the silicon surface passivation by aluminum oxide grown using a non-pyrophoric aluminum precursor, Phys. Status Solidi Rapid Res. Lett. 12 (2018), https://doi.org/10.1002/pssr.201800156.